

This discussion paper is/has been under review for the journal Atmospheric Chemistry and Physics (ACP). Please refer to the corresponding final paper in ACP if available.

Implementation of warm-cloud processes in a source-oriented WRF/Chem model to study the effect of aerosol mixing state on fog formation in the Central Valley of California

H.-H. Lee^{1,a}, S.-H. Chen¹, M. J. Kleeman², H. Zhang², S. P. DeNero², and D. K. Joe²

¹Department of Land, Air, and Water Resources, University of California, Davis, CA, USA

²Department of Civil & Environmental Engineering, University of California, Davis, CA, USA

^anow at: Singapore-MIT Alliance for Research and Technology (SMART), Centre for Environmental Sensing and Modeling (CENSAM), Singapore

Received: 19 October 2015 – Accepted: 6 November 2015 – Published: 17 November 2015

Correspondence to: S.-H. Chen (shachen@ucdavis.edu)

Published by Copernicus Publications on behalf of the European Geosciences Union.

Implementation of
warm-cloud
processes in
a source-oriented
WRF/Chem model

H.-H. Lee et al.

Title Page

Abstract

Introduction

Conclusions

References

Tables

Figures

◀

▶

◀

▶

Back

Close

Full Screen / Esc

Printer-friendly Version

Interactive Discussion

Abstract

The source-oriented Weather Research and Forecasting chemistry model (SOWC) was modified to include warm cloud processes and applied to investigate how aerosol mixing states influence fog formation and optical properties in the atmosphere. SOWC tracks a 6-dimensional chemical variable (X , Z , Y , Size Bins, Source Types, Species) through an explicit simulation of atmospheric chemistry and physics. A source-oriented cloud condensation nuclei module was implemented into the SOWC model to simulate warm clouds using the modified two-moment Purdue Lin microphysics scheme. The Goddard shortwave and longwave radiation schemes were modified to interact with source-oriented aerosols and cloud droplets so that aerosol direct and indirect effects could be studied.

The enhanced SOWC model was applied to study a fog event that occurred on 17 January 2011, in the Central Valley of California. Tule fog occurred because an atmospheric river effectively advected high moisture into the Central Valley and nighttime drainage flow brought cold air from mountains into the valley. The SOWC model produced reasonable liquid water path, spatial distribution and duration of fog events. The inclusion of aerosol–radiation interaction only slightly modified simulation results since cloud optical thickness dominated the radiation budget in fog events. The source-oriented mixture representation of particles reduced cloud droplet number relative to the internal mixture approach that artificially coats hydrophobic particles with hygroscopic components. The fraction of aerosols activating into CCN at a supersaturation of 0.5% in the Central Valley decreased from 94% in the internal mixture model to 80% in the source-oriented model. This increased surface energy flux by 3–5 W m⁻² and surface temperature by as much as 0.25 K in the daytime.

Implementation of warm-cloud processes in a source-oriented WRF/Chem model

H.-H. Lee et al.

Title Page

Abstract

Introduction

Conclusions

References

Tables

Figures

◀

▶

◀

▶

Back

Close

Full Screen / Esc

Printer-friendly Version

Interactive Discussion



1 Introduction

Atmospheric aerosols are complex mixtures of particles emitted from many different anthropogenic and natural sources suspended in the atmosphere. In contrast to greenhouse gases, aerosols have large spatial and temporal variability in the troposphere because of their short lifetimes (about one week) before coagulation, dry deposition, or wet scavenging processes remove them from the atmosphere (Ramanathan et al., 2001). Aerosol particles can influence human health (McMichael et al., 2006), ecological health (over land and ocean) (Griffin et al., 2001), visible range through the atmosphere (Dick et al., 2000), cloud/precipitation formation (Chen et al., 2008), and the net radiation budget of the earth (IPCC, 2007). Some chemical components of aerosol particles are important to direct radiative forcing of the climate due to their optical properties (Tegen et al., 1996). Particulate sulfate scatters incoming solar radiation, leading to an estimated direct forcing of -0.95 W m^{-2} (Adams et al., 2001). Particulate black carbon strongly absorbs incoming shortwave radiation, which warms the mid-level of the atmosphere but cools the earth's surface (Yang et al., 2009; Koch and Del Genio, 2010). Particulate black carbon also leads to reduce relative humidity and cloud liquid water content (semi-direct effect) in the mid-level atmosphere (Ackerman et al., 2000; Koch and Del Genio, 2010). In addition to these direct effects, Twomey (1974) proposed that aerosols indirectly affect the earth's energy budget due to their ability to serve as cloud condensation nuclei (CCN), which are of great importance in cloud development, especially for warm clouds in the mid-to-high latitudes. Large numbers of CCN produce clouds with a greater number of smaller size cloud droplets (Chen et al., 2008). These smaller cloud droplets raise cloud albedo (the first indirect effect) and also suppress the formation of precipitation and prolong cloud lifetime (the second indirect effect) (Albrecht, 1989). The direct, semi-direct, and indirect effects of aerosol particles modify the energy budgets in the atmosphere and on the surface, with corresponding changes in atmospheric stability. The 2007 IPCC report (IPCC, 2007) concluded that the net forcing of all aerosols could be either positive or negative in the range from

Implementation of warm-cloud processes in a source-oriented WRF/Chem model

H.-H. Lee et al.

Title Page

Abstract

Introduction

Conclusions

References

Tables

Figures



Back

Close

Full Screen / Esc

Printer-friendly Version

Interactive Discussion



Implementation of warm-cloud processes in a source-oriented WRF/Chem model

H.-H. Lee et al.

Title Page

Abstract

Introduction

Conclusions

References

Tables

Figures

◀

▶

◀

▶

Back

Close

Full Screen / Esc

Printer-friendly Version

Interactive Discussion



and other aerosol types) and 8 size bins. The initial particle sizes from emissions are 0.005, 0.1105, 0.221, 0.4415, 0.8835, 1.767, 3.535, and 7.0693 microns. Note that the SOWC model uses moving size bins whose sizes change in response to gas-particle conversion during model simulations. The model conserves aerosol mass concentration throughout the simulation of atmospheric processes including emissions, transport, deposition, coagulation, and condensation/evaporation. The gas-phase species emitted from different sources in each grid cell are not tracked separately in the SOWC model at the present time. In the current study, the initial and boundary conditions of aerosol particles are based on observations from the California Regional Particulate Air Quality Study (CRPAQS) (Ying et al., 2008). The distribution of particle emissions for different bins for every source are calculated using emissions inventories provided by the California Air Resources Board (CARB) along with measured chemical speciation profiles (Ying et al., 2008). Further details of the SOWC model structure and source-oriented chemistry processes are described by Zhang et al. (2014) and Joe et al. (2014).

2.2 Cloud microphysics scheme

The original Purdue Lin microphysics scheme was designed as a one-moment water mass conserved microphysics scheme with five hydrometeors: cloud water, rain, cloud ice, snow, and graupel (Lin et al., 1983; Chen and Sun, 2002). Chapman et al. (2009) added a prognostic treatment of cloud droplet number (Ghan et al., 1997) to the Purdue Lin scheme to make a two-moment treatment of cloud water within WRF/Chem. In our study, a source-oriented CCN module was added to the SOWC model to track size-resolved information about activated CCN from various aerosol sources. A new source-oriented 6-D cloud variable, “CLDAQC” (X , Z , Y , Size Bins, Source Types, Species) was added to SOWC to describe source-oriented clouds. Droplet radius and number concentration are once again stored as the last two elements in the species dimension of the CLDAQC variable. In the Purdue Lin scheme, all microphysics processes are parameterized with water mass, except autoconversion. Chapman et al. (2009)

added the autoconversion parameterization from Liu et al. (2005) into the Purdue Lin microphysics, which depends on cloud droplet number. Chapman et al. (2009) also specified changes to cloud droplet number proportional to the microphysics process rate of cloud water mass. For example, when 10 % cloud water becomes rain water after autoconversion, 10 % cloud droplets will be moved at the same time.

The continuity equation of the mass-coupled mixing ratio of CLDAQC can be written as follows:

$$\frac{\partial \text{CLDAQC}}{\partial t} = \nabla \cdot \mathbf{V} \text{CLDAQC} + \nabla \cdot K \nabla \text{CLDAQC} + P_{\text{AACT}} + S_{\text{micro}}, \quad (1)$$

where \mathbf{V} is the 3-D wind vector and K is the eddy diffusion coefficient. The first two terms on the right hand side of Eq. (1) are the flux divergence of CLDAQC (transport) and sub-grid eddy mixing, respectively. Figure 1 shows the schematic diagram of the sinks and sources of CLDAQC in the cloud microphysics processes (P_{AACT} and S_{micro}). Aerosol activation (P_{AACT}) is the main source of CLDAQC. The calculation of aerosol activation is based on a maximum supersaturation determined from a Gaussian spectrum of updraft velocities and aerosol chemistry composition for each size bin (Abdul-Razzak and Ghan, 2002). This parameterization of aerosol activation was implemented in WRF/Chem model (Chapman et al., 2009) and is used in this study. Aerosol activation was calculated each time step. Once the environment reached the critical supersaturation, AQC activated as CCN. Water vapor condenses at a diffusion limited rate to cloud droplets (water molecules transferred from vapor to cloud in Purdue Lin scheme) and particle mass/number is transferred from the interstitial aerosol variable (AQC) to the cloud-borne aerosol variable (CLDAQC). The Purdue Lin microphysics scheme uses a saturation adjustment approach (i.e., it adjusts water vapor to the saturation mixing ratio), so CCN activation is calculated before saturation adjustment. After saturation adjustment, the condensation rate due to vapor diffusion is proportional to particle size (Rogers and Yau, 1989). Results from CCN activation tests at relevant supersaturation are discussed in Sect. 4.3.

Implementation of warm-cloud processes in a source-oriented WRF/Chem model

H.-H. Lee et al.

Title Page

Abstract

Introduction

Conclusions

References

Tables

Figures

◀

▶

◀

▶

Back

Close

Full Screen / Esc

Printer-friendly Version

Interactive Discussion



Implementation of warm-cloud processes in a source-oriented WRF/Chem model

H.-H. Lee et al.

Title Page

Abstract

Introduction

Conclusions

References

Tables

Figures

◀

▶

◀

▶

Back

Close

Full Screen / Esc

Printer-friendly Version

Interactive Discussion



Sinks and sources of CLDAQC (S_{micro}) are based on interactions between a cloud droplet and the other hydrometeors (e.g., ice, rain, snow, and graupel) that can remove water from or add water to CLDAQC. The sinks of cloud water, as well as CLDAQC, include autoconversion from cloud to rain (P_{RAUT}) and the accretion of cloud water by rain (P_{RACW}), snow (P_{SACW}), and graupel (P_{GACW}). The exchange between cloud water and cloud ice can also occur through homogenous freezing of cloud water to ice (P_{IHOM}) and melting of cloud ice to cloud water (P_{IMLT}). Finally, the condensation (associated with P_{ACCT}) and evaporation of cloud water (P_{CEVP}) are implicitly taken into account in the Purdue Lin microphysics scheme. When cloud droplets fully evaporate (sink of CLDAQC), the residual cores are released back into the corresponding source type and size bin of the aerosol (AQC) variable.

2.3 Radiation schemes

The NASA Goddard shortwave and longwave radiation schemes (Chou and Suarez, 1999b, 2001b) are used in conjunction with the source-oriented cloud droplet algorithms in the enhanced SOWC model. Absorption of radiation by water vapor, ozone, oxygen, carbon dioxide, cloud droplets and aerosol particles is considered. Interactions among the absorption and scattering by clouds and aerosols (Mie scattering), molecules (Rayleigh scattering) and the surface are fully accounted for (Skamarock et al., 2008). Three main optical parameters are calculated for each model layer to describe the influence of aerosols on the radiation: aerosol optical thickness (τ), single scattering albedo (ω), and asymmetry factor (g). In the present study, the numerical code described by Ying and Kleeman (2003) was implemented to calculate the optical properties of source-oriented particles. The original numerical code of Mie scattering developed by Bohren and Huffman (1983) was used to calculate the particle extinction efficiency, scattering efficiency and asymmetry factor. The partial molar refractive index approach described in Stelson (1990) was used to estimate the mean refractive index for multi-component aerosols.

For any wavelength of shortwave or longwave radiation (λ), the aerosol optical thickness (τ_a) of a model layer with depth h (m) containing a number concentration $n_a(r)$ ($\# \text{m}^{-3} \mu\text{m}^{-1}$) of droplets with radius r (μm) is given by

$$\tau_a(\lambda) = \pi h \int_0^{\infty} Q_e(\lambda, r) r^2 n_a(r) dr, \quad (2)$$

5 where, Q_e is the dimensionless extinction efficiency. The equivalent definition of aerosol optical thickness for discrete size bins j with a mean radius r_j (μm) can be written as

$$\tau_a(\lambda) = \pi h \sum_i^n \sum_j^m Q_{ei,j}(\lambda, r) r_{i,j}^2 N_{i,j}, \quad (3)$$

10 where subscript i refers to emission source, subscript j refers to size, n is the number of particle source types and m is the number of particle sizes. N ($\# \text{m}^{-3}$) is the number of particles. The mean asymmetry factor (g_a) and single scattering albedo (ω_a) are calculated using the method described in (Yang, 2000):

$$g_a(\lambda) = \frac{\sum_i^n \sum_j^m Q_{si,j}(\lambda, r) g_{i,j}(\lambda, r) N_{i,j} \pi r_{i,j}^2}{\sum_i^n \sum_j^m Q_{si,j}(\lambda, r) N_{i,j} \pi r_{i,j}^2}, \quad (4)$$

$$\omega_a(\lambda) = \frac{\sum_i^n \sum_j^m Q_{si,j}(\lambda, r) N_{i,j} \pi r_{i,j}^2}{\sum_i^n \sum_j^m Q_{ei,j}(\lambda, r) N_{i,j} \pi r_{i,j}^2}, \quad (5)$$

15 where Q_s is the dimensionless scattering efficiency. All of the optical parameters are functions of the wavelength (λ) of incident radiation.

In the original Goddard radiation schemes, cloud droplets are assigned to a mono-disperse size distribution (mean effective radius) which depends on the water mass and

5 sipating from the northern Central Valley on 18 January and fully dissipated on 19 January (Fig. 2c).

10 In addition to calm wind and radiative cooling, high moisture is an important ingredient to a Tule fog event in the Central Valley, California. Figure 3 shows the time series of column integrated water vapor, sea level pressure, and 850 hPa wind vectors from ECMWF Interim reanalysis data. On 11 January, the column water vapor (CWV) was very low, less than 10 mm, over the Central Valley (Fig. 3a). Moisture was advected into the Central Valley (Fig. 3b) by a winter cyclone moving close to the northwestern coast of the United States on 12 January. A weak southwest-northeast-oriented atmospheric river with a width of 1000 km and a maximum CWV of ~ 26 – 28 mm approached the western coast and brought moisture into the Central Valley. At 00:00 UTC, 13 January (Fig. 3c), moisture content began increasing in the northern Central Valley. At night, drainage flow from the surrounding mountains brought cold air into the Central Valley, mixed with the low-level moist air, and initiated fog formation over the northern Central Valley. On 14 January (Fig. 3d), the CWV over the southern Central Valley reached 22–24 mm and fog formed over the southern Central Valley.

15 On 15 and 16 January, a more intense, west-southwest to east-northeast oriented atmospheric river advected moisture into northern California (Fig. 3e and f). The moisture in the Central Valley reached a maximum on 17 January (Fig. 3g), at the time when the fog reached its maximum thickness during the study period (Fig. 2; also see the cloud optical thickness discussion later). On 18 January (Fig. 3h), while high moisture and fog still presented over the southern Central Valley, the moisture decreased and the fog disappeared over the northern Central Valley. Fog fully dissipated in the Central Valley on 19 January.

20 According to the satellite images and surface temperature variation, the coverage and thickness of fog followed a diurnal pattern with thinning in the daytime and thickening at night. As mentioned earlier, the aerosol mixture state can impact fog formation and properties of cloud droplets.

Implementation of warm-cloud processes in a source-oriented WRF/Chem model

H.-H. Lee et al.

Title Page	
Abstract	Introduction
Conclusions	References
Tables	Figures
◀	▶
◀	▶
Back	Close
Full Screen / Esc	
Printer-friendly Version	
Interactive Discussion	



3.2 Observational data

Multiple types of measurement data were used to evaluate the SOWC model performance. MODIS level 2 cloud products from the Terra and Aqua satellites provide 5 km resolution cloud optical thickness (COT) and liquid water path (LWP). The LWP retrieval from MODIS has been used to study low cloud and fog (Bendix et al., 2005). High-resolution MODIS data can describe fog spatial distribution and intensity but are only available once every 24 h (daytime only) from each satellite. The SOWC model predictions for temperature and moisture at the surface are also evaluated against in situ time-series meteorological data from 24 surface weather stations along with net ground shortwave fluxes at 42 sites from California Irrigation Management Information System (CIMIS). Measured concentrations of airborne particles were obtained from the California Ambient Air Quality Data (CAAQD) provided by the Planning and Technical Support Division (PTSD) of the California Air Resources Board (CARB). The station details of CAAQD are provided in Table 2. The locations of all measurement sites are provided in Fig. 4.

3.3 Numerical experiment design

The primary objective of this study is to examine how the source-oriented ($S_{_}$) and internal ($I_{_}$) mixture representations of aerosol particles differ in their feedbacks to meteorology in a fog event. Internally mixed simulations ($I_{_}$) artificially blend emissions from all sources into a single particle size distribution thereby concealing all advanced treatments of particle mixing and aging. Four experiments were carried out (Table 3) for the selected fog event. In the basecase experiment of S_ARon_CRmod the polluted aerosol particles tracked by AQC act as the source of CCN ($S_{_}$) and the aerosol–radiation interaction (aerosol direct effect) is enabled in the radiation schemes ($ARon$). The geometric-optics approach mentioned in Sect. 2.3 is used to calculate the cloud optical properties of each model layer ($CRmod$). S_ARon_CRorig is similar to S_ARon_CRmod , except for the use of the original cloud optical property calculation

**Implementation of
warm-cloud
processes in
a source-oriented
WRF/Chem model**

H.-H. Lee et al.

Title Page

Abstract

Introduction

Conclusions

References

Tables

Figures

◀

▶

◀

▶

Back

Close

Full Screen / Esc

Printer-friendly Version

Interactive Discussion

(CRorig) in the NASA Goddard shortwave and longwave radiation schemes. As discussed previously, the original schemes are based on an estimate of the cloud droplet effective radius using the cloud mass and number concentration (CRorig). The radius of cloud droplets in the original Goddard shortwave radiation scheme is constrained to the range from 4 to 20 μm . In the modified cloud–radiation scheme (CRmod), the size range of cloud droplets in Eq. (3) can vary between the dry aerosol particle radius to 30 μm . S_ARoff_CRmod has no aerosol direct effect in the radiation schemes (ARoff). The comparison of S_ARoff_CRmod and S_ARon_CRmod is used to estimate the aerosol direct effect in this study.

Each numerical experiment employed two domains with two-way nesting. Domain 1 (86 \times 97 grid cells) had a resolution of 12 km while domain 2 (127 \times 202 grid cells) had a resolution of 4 km. Domain 2 was positioned to cover the entire Central Valley of California and results from this domain are used for the subsequent analysis. All simulations used 31 vertically staggered layers based on a terrain-following pressure coordinate system. The vertical layers are stretched with a higher resolution near the surface (an average depth of \sim 30 m in the first model half layer). Variables other than vertical velocity and geopotential were stored in the half model levels. The time step was 60 s for the first domain and 20 s for the second domain. The physics schemes employed for the simulations included the modified Purdue Lin microphysics scheme (Chen and Sun, 2002), the NASA Goddard longwave/shortwave radiation schemes (Chou and Suarez, 1999a, 2001a), the Kain-Fritsch cumulus scheme (Kain and Fritsch, 1990; Kain, 1993) (domain 1 only), the YSU PBL scheme (Hong et al., 2006; Hong, 2010) and the Noah LSM surface scheme (Tewari et al., 2007). The number of cloud droplets was not considered in the convective scheme in the SOWC model. The target episode had calm winds with local fog formation in the Central Valley (not propagating in through lateral boundaries). Moreover, the event occurred in the winter season when the Convective Available Potential Energy (CAPE) was small. Therefore, the KF cumulus convective parameterization is inactive for this cases study. The meteorological initial and bound-

ary conditions were taken from North American Regional Reanalysis (NARR), which has a spatial resolution of 32 km and a temporal resolution of 3 h.

The SOWC model tracked two 6-D variables for aerosol/cloud properties which introduce considerable computational burden for model simulations when compared to standard WRF/Chem model simulation (with prescribed aerosol concentration). The computational cost of the SOWC model, which is proportional to the extra information that is tracked, is approximately 25 times higher than that of the standard WRF/Chem simulation in the current study. SOWC model simulations started at 00:00 UTC 9 January (7 days prior to the start of the thick fog event) with four-dimensional data assimilation (FDDA). This approach provides a realistic heterogeneous aerosol distribution and low-level temperature and moisture fields at the start of the thick fog simulation. Observations from surface stations and NARR data were used for nudging during this aerosol spin-up period. Between 00:00 UTC 16 January to 00:00 UTC 19 January, the SOWC model integrated without FDDA (3 day free run) during which time the effects of the different model configurations were observed and is our major interested time period.

4 Model results

4.1 Evaluation of basecase (S_ARon_CRmod) model performance

The SOWC model calculates CCN number concentrations based on the activation of aerosols (AQC). The AQC number concentration can influence the intensity of initial fog formation and spatial distribution of final fog fields, and thus AQC number concentration is examined first. Figure 5 shows 72 h averaged (from 16 to 18 January 2011) AQC number concentrations in California's Central Valley that were also averaged over the first five model layers for S_ARon_CRmod. Fog usually forms within the planet boundary layer (PBL), which reaches to a height of approximately five model layers in winter conditions in the Central Valley (450–550 m). Temporally averaged AQC concentrations

Implementation of warm-cloud processes in a source-oriented WRF/Chem model

H.-H. Lee et al.

Title Page

Abstract

Introduction

Conclusions

References

Tables

Figures

◀

▶

◀

▶

Back

Close

Full Screen / Esc

Printer-friendly Version

Interactive Discussion



are approximately $2 \times 10^9 \# m^{-3}$, with the highest concentrations predicted in the vicinity of polluted cities (e.g., the San Francisco Bay Area, Stockton, Modesto, Sacramento, Fresno, and Bakersfield), in the middle of the Central Valley, and at foothills of Sierra Nevada Mountain over the east-southeastern Central Valley.

Figure 6 shows the comparison of simulated nitrate (NO_3^-), sulfate (SO_4^{2-}), ammonium (NH_4^+) and soluble sodium (Na^+) concentrations to measured values at 6 monitoring stations (see Table 2 and Fig. 4) on 18 January 2011. Simulated sulfate and soluble sodium are in reasonable ($> 80\%$) agreement with measurements but nitrate and ammonium concentrations were under predicted by approximately 70%. The cause for this discrepancy is unknown, but one possibility is the presence of organic nitrate compounds in the atmosphere that are not simulated by the model chemistry. Note that both observed and predicted nitrate concentrations in the current episode are lower than the maximum concentrations observed in historical extreme episodes within the San Joaquin Valley (SJV) because the current stagnation event only lasted a few days while extreme events last multiple weeks. The S_ARon_CRmod experiment reasonably reproduces the observed spatial distribution and magnitude of liquid water path (LWP) compared to the data retrieved from MODIS (Fig. 7). In particular, the model predicts LWP well over the northern portion of the Central Valley during the fog event (16 to 18 January). However, the model under-predicts LWP in the middle portion of the Central Valley, which caused the fog to dissipate earlier (late 17 January). For the southern portion of the Central Valley, the fog event starts earlier (14 to 15 January) and the model reasonably predicts the onset of the event. But the simulated fog is too dense (figure not shown). In addition, the peak of the simulated fog occurs one day earlier (16 January forecast vs. 17 January observed). This timing difference could be caused by the change in the microphysics processes at 00:00 UTC 16 January. During the FDDA time period (before 16 January), the one-moment bulk microphysics scheme is used. After the FDDA time period, aerosols start being involved in cloud formation. High Nitrate concentrates in the SJV and enhances aerosol activation due to its high

Implementation of warm-cloud processes in a source-oriented WRF/Chem model

H.-H. Lee et al.

Title Page

Abstract

Introduction

Conclusions

References

Tables

Figures

◀

▶

◀

▶

Back

Close

Full Screen / Esc

Printer-friendly Version

Interactive Discussion



**Implementation of
warm-cloud
processes in
a source-oriented
WRF/Chem model**

H.-H. Lee et al.

Title Page

Abstract

Introduction

Conclusions

References

Tables

Figures

◀

▶

◀

▶

Back

Close

Full Screen / Esc

Printer-friendly Version

Interactive Discussion

deviation from 24 surface stations in the daytime and nighttime of S_ARoff_CRmod are similar to, but larger than, results from S_ARon_CRmod for $T2$ and $Q2$ at the ground. However, compared to S_ARon_CRmod, the smaller cold bias from S_ARoff_CRmod is consistent with its larger net downward shortwave radiative flux (NSF) shown in Tables 4 and 5. Table 5 shows that the average NSF within the entire Central Valley from S_ARoff_CRmod is higher than S_ARon_CRmod by 3.7 W m^{-2} , which means that aerosol radiative forcing the shortwave energy flux reaching the ground reduces by $\sim 3.7 \text{ W m}^{-2}$ in this case study. The maximum increases of $T2$ and NSF by the aerosol direct effect occurred on 17 January 2011 (Fig. 9). Table 5 also shows the mean value of cloud water mixing ratio, cloud droplet number, surface skin temperature, latent heat flux and sensible heat flux over the Central Valley during 16 to 18 January 2011. Cloud water mixing ratio and cloud droplet number were averaged within the first five model layers. The aerosol direct effect leads to increases in the cloud water mass and cloud droplet number by 3.3 and 4.5 %, respectively, due to reductions in skin temperature (0.1 K) and net shortwave flux (3.7 W m^{-2}).

The modified radiation schemes for cloud optical properties in the S_ARon_CRmod experiment do not have significant feedback on spatially and temporally averaged cloud water mass and cloud droplet number (i.e., compared to S_ARon_CRorig) as shown in Table 5. Theoretically, the modified cloud–radiation interaction (i.e., geometric-optics method) used in the COT calculations (S_ARon_CRmod) can predict higher COT which leads to slightly lower net shortwave flux and surface skin temperature, especially in the polluted area. The higher COT predictions are likely caused by differences in the size range of cloud droplets and refractive indexes of cloud water with/without chemical composition in the calculation of cloud radiative properties. As mentioned above, the radius of cloud droplets in the original Goddard shortwave radiation scheme is constrained to the range from 4 to $20 \mu\text{m}$, while in our modified radiation scheme, the cloud droplets are allowed to range in size between the dry aerosol particle radius to $30 \mu\text{m}$. The parameterization of cloud optical thickness in the original Goddard radiation scheme assumes that cloud droplets are pure water. The modified scheme recognizes

Implementation of warm-cloud processes in a source-oriented WRF/Chem model

H.-H. Lee et al.

Title Page

Abstract

Introduction

Conclusions

References

Tables

Figures

◀

▶

◀

▶

Back

Close

Full Screen / Esc

Printer-friendly Version

Interactive Discussion



the chemical species in the cloud water and considers these species when calculating the cloud droplet index of refraction. However, in this case study the results of these two experiments (i.e., S_ARon_CRmod and S_ARon_CRorig) were very similar. Because the meteorological conditions of the fog event are calm and stable, the cloud microphysics processes are fairly slow and simple (no rain produced in this case). The size distribution of cloud droplets were virtually identical in the original and modified radiation schemes, but S_ARon_CRorig had slightly cloud droplet number concentrations (Table 5).

4.3 Internal mixture vs. source-oriented aerosols

The mixing state of chemical components among the atmospheric aerosol particles can potentially play an important role in fog formation. The activation of aerosol particles into cloud droplets depends on the critical super-saturation which in turn depends on particle composition. According to the Köhler equation, increased concentrations of solutes will decrease the critical super-saturation required to activate a particle into a CCN. As mentioned earlier, hydrophobic particles (i.e. black carbon) will more easily serve as CCN once they are coated with hygroscopic material (i.e. sulfate). Increased concentrations of solutes can potentially modify the frequency and severity of fog events in polluted air. In this section, we compare results from S_ARon_CRmod (source-oriented experiment) and I_ARon_CRmod (internally mixed experiment) to investigate the activation change and further meteorological responses between internally mixed and source-oriented aerosols. The internally mixed experiment is conducted by lumping all sources together (i.e., AQC source dimension collapsed to one producing a 5-D AQC variable).

It is likely that the ratio of CCN concentration (N_{CCN}) to total aerosol concentration (N_{CN}) will be different for each of the five source types tracked in S_ARon_CRmod since the CCN activation depends on the chemical composition and size of the particles. The highest ratio of N_{CCN}/N_{CN} for S_ARon_CRmod and I_ARon_CRmod is located in the southern Central Valley (Fig. 10) due to higher moisture from the at-

**Implementation of
warm-cloud
processes in
a source-oriented
WRF/Chem model**

H.-H. Lee et al.

Title Page

Abstract

Introduction

Conclusions

References

Tables

Figures

◀

▶

◀

▶

Back

Close

Full Screen / Esc

Printer-friendly Version

Interactive Discussion

mospheric river resulting in greater aerosols activation to CCNs and smaller residual aerosol number concentration (see Fig. 5). Over the Central Valley during 16 to 18 January 2011, the ratio of $N_{\text{CCN}}/N_{\text{CN}}$ for each source type is 12.63, 15.60, 14.89, 16.80 and 20.21 % for wood smoke, gasoline, diesel, meat cooking, and others, respectively (averaged within the first five model layers). Wood smoke is typically a major source of aerosol ($\sim 38\%$) in California's Central Valley during winter stagnation events (see Table 6) and the organic carbon in wood smoke is water-soluble (Dusek et al., 2011) which allows these particles to activate more easily than insoluble particles. However, the majority of the wood smoke particles are located in the smallest size bin, so the ratio of $N_{\text{CCN}}/N_{\text{CN}}$ for wood smoke is comparable with that of hydrophobic diesel. The source type of "others", which has the highest ratio of $N_{\text{CCN}}/N_{\text{CN}}$, is dominated by larger dust particles coated with secondary components such as nitrate and are easier to activate, in contrast to the smaller combustion particles emitted from other tracked sources.

The comparison of the average ratio of $N_{\text{CCN}}/N_{\text{CN}}$ from the first five model layers between S_ARon_CRmod and I_ARon_CRmod is shown on Fig. 10. The spatial patterns produced by both experiments are similar but I_ARon_CRmod has a higher $N_{\text{CCN}}/N_{\text{CN}}$ ratio, in particular over the northern two thirds of the Central Valley. The largest differences between $N_{\text{CCN}}/N_{\text{CN}}$ predicted by S_ARon_CRmod and I_ARon_CRmod occur in regions with large emissions of wood smoke (figure not shown). The ratio of $N_{\text{CCN}}/N_{\text{CN}}$ for both experiments can reach $> 30\%$ but the highest $N_{\text{CCN}}/N_{\text{CN}}$ ratio occurs in relatively less polluted regions. The spatially averaged ratio of $N_{\text{CCN}}/N_{\text{CN}}$ is 16.65 % for S_ARon_CRmod and 27.49 % for I_ARon_CRmod within the Central Valley over the period of 16 to 18 January. The CCN concentrations and $N_{\text{CCN}}/N_{\text{CN}}$ ratios between internally mixed and source-oriented experiments at different super-saturations were calculated to better understand this result. Figure 11a shows the 72h averaged CCN concentration at super-saturations of 0.02, 0.05, 0.1, 0.2 and 0.5 % and total AQC concentration averaged within the first five model layers. Figure 11b presents corresponding $N_{\text{CCN}}/N_{\text{CN}}$ ratios at 5 different super-saturations.

**Implementation of
warm-cloud
processes in
a source-oriented
WRF/Chem model**

H.-H. Lee et al.

Title Page

Abstract

Introduction

Conclusions

References

Tables

Figures

◀

▶

◀

▶

Back

Close

Full Screen / Esc

Printer-friendly Version

Interactive Discussion

Valley (Fig. 12a). The largest relative change in predicted cloud water concentration also occurs in the northern Central Valley near the mountains where fogs are initiated by drainage flow. I_ARon_CRmod predicts higher cloud droplet number (Fig. 12b), with the largest relative increases (~ 50 – 60%) once again observed in areas near mountains and highly polluted regions with more modest changes of $20 \sim 30\%$ over remote regions. Internally mixed aerosols reduce the critical saturation ratio for particles by artificially mixing hygroscopic and hydrophobic components that in turn allows particles to activate more easily.

The internally mixed experiment (I_ARon_CRmod) predicts lower daytime averaged surface skin temperature and net downward shortwave flux at ground (Fig. 12c and d) corresponding to the areas with higher cloud water mixing ratio and cloud droplet concentrations (Fig. 12a and b). This result is expected since higher cloud water mixing ratio and cloud droplet concentration will reduce the solar radiation flux on the surface. The reduction of surface skin temperature in the internal mixed experiment is proportional to the change of the net shortwave radiation. Figure 13 shows that the area average of latent heat flux (LH) and sensible heat flux (SH) over the Central Valley in S_ARon_CRmod and the average difference of internally mixed and source-oriented experiments. Higher cloud amount and lower surface temperature are predicted in the internally mixed experiment leading to reduced LH and SH fluxes at ground level compared to the source-oriented experiment. The difference between internally mixed and source-oriented predictions for LH and SH reached 3 and 5 W m^{-2} , respectively, at noon local time (22:00 UTC 17 January).

Table 7 shows hourly mean bias and root-mean-square-difference between internally mixed (I_ARon_CRmod) and source-oriented (S_ARon_CRmod) experiments for six variables within the Central Valley during 16 to 18 January 2011. The mean bias between these two experiments is $1.19 \times 10^{-2} \text{ (g m}^{-3}\text{)}$ for cloud water mixing ratio and $6.24 \times 10^7 \text{ (# m}^{-3}\text{)}$ for cloud droplet number. The direction of these trends is expected since internally mixed aerosols are easier to activate as CCN. The mean bias between internally mixed and source-oriented experiments is -0.15 (K) for surface skin temper-

ature and -6.02 (W m^{-2}) for net shortwave flux. The mean bias of LH and SH is -0.61 and -0.36 (W m^{-2}), respectively. The root-mean-square-difference between these two experiments is large for each variable, meaning that the difference varies strongly with location (see Fig. 12).

5 Summary and discussion

A warm cloud-aerosol interaction module was implemented into the source-oriented Weather Research and Forecasting model with Chemistry (SOWC) to study the aerosol–cloud–radiation interactions during fog simulations. The source-oriented mixture of aerosols is used to explicitly simulate particle aging processes in the atmosphere rather than instantaneously combining particles into an internal mixture. The SOWC model was used to simulate a fog event in California’s Central Valley in January 2011 with seven days of FDDA nudging and three days of free run. Fog formation occurred when high moisture content from an Atmospheric River was advected into the Central Valley and cold drainage flows occurred into the valley at night. The initial tests used 5 emissions sources (wood smoke, gasoline, diesel, meat cooking, and others) with particles from each source consisting of 38 chemical species and 8 size bins, spanning a diameter range from 0.01 to 10 microns. The highest model spatial resolution was 4 km.

Four numerical experiments were conducted to test model performance, meteorological feedbacks from internal and source-oriented aerosols, and the impact of aerosol–cloud–radiation interaction on fog formation. Compared to observations, the SOWC model reasonably predicted fog spatial distribution and duration and environmental meteorological feedbacks. However, the model over-predicted liquid water path and cloud optical thickness, which resulted in cold surface temperature bias. The inclusion of aerosol–radiation interaction reduced net downward shortwave radiative flux by an average of 3.7 W m^{-2} and daytime surface temperature by 0.1 K. Results that used different treatments for aerosol mixing states were compared, and the important findings

Implementation of warm-cloud processes in a source-oriented WRF/Chem model

H.-H. Lee et al.

Title Page

Abstract

Introduction

Conclusions

References

Tables

Figures

◀

▶

◀

▶

Back

Close

Full Screen / Esc

Printer-friendly Version

Interactive Discussion



References

- Abdul-Razzak, H. and Ghan, S. J.: A parameterization of aerosol activation 3. Sectional representation, *J. Geophys. Res.-Atmos.*, 107, AAC 1–1–AAC 1–6, doi:10.1029/2001jd000483, 2002.
- 5 Ackerman, A. S., Toon, O. B., Stevens, D. E., Heymsfield, A. J., Ramanathan, V., and Welton, E. J.: Reduction of Tropical Cloudiness by Soot, *Science*, 288, 1042–1047, doi:10.1126/science.288.5468.1042, 2000.
- Ackermann, I. J., Hass, H., Memmesheimer, M., Ebel, A., Binkowski, F. S., and Shankar, U.: Modal aerosol dynamics model for Europe: development and first applications, *Atmos. Environ.*, 32, 2981–2999, doi:10.1016/S1352-2310(98)00006-5, 1998.
- 10 Adams, P. J., Seinfeld, J. H., Koch, D., Mickley, L., and Jacob, D.: General circulation model assessment of direct radiative forcing by the sulfate-nitrate-ammonium-water inorganic aerosol system, *J. Geophys. Res.-Atmos.*, 106, 1097–1111, doi:10.1029/2000jd900512, 2001.
- Albrecht, B. A.: Aerosols, Cloud Microphysics, and Fractional Cloudiness, *Science*, 245, 1227–1230, doi:10.1126/science.245.4923.1227, 1989.
- 15 Bendix, J., Thies, B., Cermak, J., and Nauß, T.: Ground fog detection from space based on MODIS daytime data—a feasibility study, *Weather Forecast.*, 20, 989–1005, 2005.
- Binkowski, F. S. and Shankar, U.: The Regional Particulate Matter Model: 1. Model description and preliminary results, *J. Geophys. Res.-Atmos.*, 100, 26191–26209, doi:10.1029/95jd02093, 1995.
- 20 Bohren, C. F. and Huffman, D. R.: *Absorption and Scattering of Light by Small Particles*, Wiley, New York, USA, 1983.
- Bott, A. and Carmichael, G. R.: Multiphase chemistry in a microphysical radiation fog model – a numerical study, *Atmos. Environ. A.-Gen.*, 27, 503–522, doi:10.1016/0960-1686(93)90208-G, 1993.
- 25 Chapman, E. G., Gustafson Jr., W. I., Easter, R. C., Barnard, J. C., Ghan, S. J., Pekour, M. S., and Fast, J. D.: Coupling aerosol–cloud–radiative processes in the WRF-Chem model: Investigating the radiative impact of elevated point sources, *Atmos. Chem. Phys.*, 9, 945–964, doi:10.5194/acp-9-945-2009, 2009.
- 30 Chen, J.-P. and Lamb, D.: Simulation of cloud microphysical and chemical processes using a multicomponent framework, Part I: Description of the microphysical model, *J. Atmos. Sci.*, 51, 2613–2630, 1994.

Implementation of warm-cloud processes in a source-oriented WRF/Chem model

H.-H. Lee et al.

Title Page

Abstract

Introduction

Conclusions

References

Tables

Figures

◀

▶

◀

▶

Back

Close

Full Screen / Esc

Printer-friendly Version

Interactive Discussion



**Implementation of
warm-cloud
processes in
a source-oriented
WRF/Chem model**

H.-H. Lee et al.

Title Page

Abstract

Introduction

Conclusions

References

Tables

Figures

◀

▶

◀

▶

Back

Close

Full Screen / Esc

Printer-friendly Version

Interactive Discussion



Chen, J.-P., Hazra, A., Shiu, C.-J., Tsai, I.-C., and Lee, H.-H.: Interaction between aerosols and clouds: current understanding, in: *Recent Progress in Atmospheric Sciences: Applications to the Asia-Pacific Region*, edited by: Liou, K. N. and Chou, M.-D., World Scientific Publishing, 231–281, 2008.

5 Chen, S.-H. and Sun, W. Y.: A one-dimensional time-dependent cloud model, *J. Meteorol. Soc. Jpn.*, 80, 99–118, 2002.

Chou, M.-D. and Suarez, M. J.: A Solar Radiation Parameterization for Atmospheric Studies, NASA Tech. Rep., NASA/TM-1999-10460, 15, 1999a.

10 Chou, M. D. and Suarez, M. J.: A Solar Radiation Parameterization for Atmospheric Studies, NASA Tech. Rep., 38, 1999b.

Chou, M.-D. and Suarez, M. J.: A Thermal Infrared Radiation Parameterization for Atmospheric Studies, NASA Tech. Rep., NASA/TM-2001-104606, 19, 2001a.

Chou, M. D. and Suarez, M. J.: A Thermal Infrared Radiation Parameterization for Atmospheric Studies, NASA Tech. Rep., 55, 2001b.

15 Chow, J. C., Watson, J. G., Lowenthal, D. H., Solomon, P. A., Magliano, K. L., Ziman, S. D., and Richards, L. W.: PM_{10} and $PM_{2.5}$ compositions in California's San Joaquin Valley, *Aerosol Sci. Tech.*, 18, 105–128, doi:10.1080/02786829308959588, 1993.

20 Cubison, M. J., Ervens, B., Feingold, G., Docherty, K. S., Ulbrich, I. M., Shields, L., Prather, K., Hering, S., and Jimenez, J. L.: The influence of chemical composition and mixing state of Los Angeles urban aerosol on CCN number and cloud properties, *Atmos. Chem. Phys.*, 8, 5649–5667, doi:10.5194/acp-8-5649-2008, 2008.

Dick, W. D., Saxena, P., and McMurry, P. H.: Estimation of water uptake by organic compounds in submicron aerosols measured during the southeastern aerosol and visibility study, *J. Geophys. Res.-Atmos.*, 105, 1471–1479, 2000.

25 Dusek, U., Reischl, G. P., and Hitzenberger, R.: CCN activation of pure and coated carbon black particles, *Environ. Sci. Technol.*, 40, 1223–1230, doi:10.1021/es0503478, 2006.

Dusek, U., Frank, G. P., Massling, A., Zeromskiene, K., Iinuma, Y., Schmid, O., Helas, G., Hennig, T., Wiedensohler, A., and Andreae, M. O.: Water uptake by biomass burning aerosol at sub- and supersaturated conditions: closure studies and implications for the role of organics, *Atmos. Chem. Phys.*, 11, 9519–9532, doi:10.5194/acp-11-9519-2011, 2011.

30 Fast, J. D., Gustafson, W. I., Easter, R. C., Zaveri, R. A., Barnard, J. C., Chapman, E. G., Grell, G. A., and Peckham, S. E.: Evolution of ozone, particulates, and aerosol direct radiative

Implementation of warm-cloud processes in a source-oriented WRF/Chem model

H.-H. Lee et al.

Title Page

Abstract

Introduction

Conclusions

References

Tables

Figures

◀

▶

◀

▶

Back

Close

Full Screen / Esc

Printer-friendly Version

Interactive Discussion

forcing in the vicinity of Houston using a fully coupled meteorology-chemistry-aerosol model, *J. Geophys. Res.-Atmos.*, 111, D21305, doi:10.1029/2005jd006721, 2006.

Frank, G., Martinsson, B. G., Cederfelt, S.-I., Berg, O. H., Swietlicki, E., Wendisch, M., Yuskiewicz, B., Heintzenberg, J., Wiedensohler, A., Orsini, D., Stratmann, F., Laj, P., and Ricci, L.: Droplet formation and growth in polluted fogs, *Contrib. Atmos. Phys.*, 71, 65–85, 1998.

Georgii, H. W. and Kleinjung, E.: Relations between the chemical composition of atmospheric aerosol particles and the concentration of natural ice nuclei, *J. Rech. Atmos.*, 3, 145–156, 1967.

Ghan, S. J., Leung, L. R., Easter, R. C., and Abdul-Razzak, H.: Prediction of cloud droplet number in a general circulation model, *J. Geophys. Res.-Atmos.*, 102, 21777–21794, doi:10.1029/97jd01810, 1997.

Grell, G. A., Peckham, S. E., Schmitz, R., McKeen, S. A., Frost, G., Skamarock, W. C., and Eder, B.: Fully coupled “online” chemistry within the WRF model, *Atmos. Environ.*, 39, 6957–6975, doi:10.1016/j.atmosenv.2005.04.027, 2005.

Griffin, D. W., Kellogg, C. A., and Shinn, E. A.: Dust in the wind: long range transport of dust in the atmosphere and its implications for global public and ecosystem health, *Global Change and Human Health*, 2, 20–33, 2001.

Hayes, T. P., Kinney, J. J. R., and Wheeler, N. J. M.: California surface wind climatology, California Air Resources Board, Technical Support Division, Modeling and Meteorology Branch, 1992.

Hong, S.-Y.: A new stable boundary-layer mixing scheme and its impact on the simulated East Asian summer monsoon, *Q. J. Roy. Meteor. Soc.*, 136, 1481–1496, doi:10.1002/qj.665, 2010.

Hong, S.-Y., Noh, Y., and Dudhia, J.: A new vertical diffusion package with an explicit treatment of entrainment processes, *Mon. Weather Rev.*, 134, 2318–2341, doi:10.1175/mwr3199.1, 2006.

IPCC: Climate change 2007 – the physical science basis: working group I contribution to the fourth assessment report of the IPCC, Cambridge University Press, Cambridge, UK, 2007.

Joe, D. K., Zhang, H., DeNero, S. P., Lee, H.-H., Chen, S.-H., McDonald, B. C., Harley, R. A., and Kleeman, M. J.: Implementation of a high-resolution source-oriented WRF/Chem model at the Port of Oakland, *Atmos. Environ.*, 82, 351–363, doi:10.1016/j.atmosenv.2013.09.055, 2014.

Implementation of warm-cloud processes in a source-oriented WRF/Chem model

H.-H. Lee et al.

Title Page

Abstract

Introduction

Conclusions

References

Tables

Figures

◀

▶

◀

▶

Back

Close

Full Screen / Esc

Printer-friendly Version

Interactive Discussion



- Kain, J. S.: Convective parameterization for mesoscale models: the Kain–Fritsch scheme, the representation of cumulus convection in numerical models, *Meteor. Mon.*, 46, 165–170, 1993.
- Kain, J. S. and Fritsch, J. M.: A one-dimensional entraining/detraining plume model and its application in convective parameterization, *J. Atmos. Sci.*, 47, 2784–2802, 1990.
- Kleeman, M. J., Cass, G. R., and Eldering, A.: Modeling the airborne particle complex as a source-oriented external mixture, *J. Geophys. Res.-Atmos.*, 102, 21355–21372, doi:10.1029/97jd01261, 1997.
- Koch, D. and Del Genio, A. D.: Black carbon semi-direct effects on cloud cover: review and synthesis, *Atmos. Chem. Phys.*, 10, 7685–7696, doi:10.5194/acp-10-7685-2010, 2010.
- Lance, S., Raatikainen, T., Onasch, T. B., Worsnop, D. R., Yu, X.-Y., Alexander, M. L., Stolzenburg, M. R., McMurry, P. H., Smith, J. N., and Nenes, A.: Aerosol mixing state, hygroscopic growth and cloud activation efficiency during MIRAGE 2006, *Atmos. Chem. Phys.*, 13, 5049–5062, doi:10.5194/acp-13-5049-2013, 2013.
- Lesins, G., Chylek, P., and Lohmann, U.: A study of internal and external mixing scenarios and its effect on aerosol optical properties and direct radiative forcing, *J. Geophys. Res.-Atmos.*, 107, doi:10.1029/2001jd000973, 2002.
- Li, W. J. and Shao, L. Y.: Observation of nitrate coatings on atmospheric mineral dust particles, *Atmos. Chem. Phys.*, 9, 1863–1871, doi:10.5194/acp-9-1863-2009, 2009.
- Lin, Y.-L., Farley, R. D., and Orville, H. D.: Bulk parameterization of the snow field in a cloud model, *J. Clim. Appl. Meteorol.*, 22, 1065–1092, 1983.
- Liu, Y., Daum, P. H., and McGraw, R. L.: Size truncation effect, threshold behavior, and a new type of autoconversion parameterization, *Geophys. Res. Lett.*, 32, L11811, doi:10.1029/2005gl022636, 2005.
- Lohmann, U. and Feichter, J.: Global indirect aerosol effects: a review, *Atmos. Chem. Phys.*, 5, 715–737, doi:10.5194/acp-5-715-2005, 2005.
- McMichael, A. J., Woodruff, R. E., and Hales, S.: Climate change and human health: present and future risks, *Lancet*, 367, 859–869, 2006.
- Ming, Y. and Russell, L. M.: Organic aerosol effects on fog droplet spectra, *J. Geophys. Res.-Atmos.*, 109, D10206, doi:10.1029/2003jd004427, 2004.
- Moore, K. F., Sherman, D. E., Reilly, J. E., and Collett, J. L.: Drop size-dependent chemical composition in clouds and fogs, Part I: observations, *Atmos. Environ.*, 38, 1389–1402, doi:10.1016/j.atmosenv.2003.12.013, 2004.

**Implementation of
warm-cloud
processes in
a source-oriented
WRF/Chem model**

H.-H. Lee et al.

Title Page

Abstract

Introduction

Conclusions

References

Tables

Figures

◀

▶

◀

▶

Back

Close

Full Screen / Esc

Printer-friendly Version

Interactive Discussion



- Motoi, K.: Electron-microscope study of snow crystal nuclei, *J. Meteorol.*, 8, 151–156, 1951.
- Niu, S. J., Liu, D. Y., Zhao, L. J., Lu, C. S., Lü, J. J., and Yang, J.: Summary of a 4-year fog field study in northern Nanjing, Part 2: fog microphysics, *Pure Appl. Geophys.*, 169, 1137–1155, doi:10.1007/s00024-011-0344-9, 2012.
- 5 Ramanathan, V., Crutzen, P. J., Kiehl, J. T., and Rosenfeld, D.: Atmosphere – aerosols, climate, and the hydrological cycle, *Science*, 294, 2119–2124, doi:10.1126/science.1064034, 2001.
- Rogers, R. R. and Yau, M. K.: *A Short Course in Cloud Physics*, 3rd Edn., Butterworth Heine-
mann, 1989.
- Schell, B., Ackermann, I. J., Hass, H., Binkowski, F. S., and Ebel, A.: Modeling the formation
10 of secondary organic aerosol within a comprehensive air quality model system, *J. Geophys. Res.-Atmos.*, 106, 28275–28293, 2001.
- Skamarock, W. C., Klemp, J. B., Dudhia, J., Gill, D. O., Barker, D. M., Duda, M. G., Huang, X.-
Y., Wang, W., and Powers, J. G.: *A Description of the Advanced Research WRF Version 3*,
NCAR Technical Note, NCAR/TN-475+STR, 2008.
- 15 Stelson, A. W.: Urban aerosol refractive index prediction by partial molar refraction approach,
Environ. Sci. Technol., 24, 1676–1679, doi:10.1021/es00081a008, 1990.
- Sullivan, R. C., Petters, M. D., DeMott, P. J., Kreidenweis, S. M., Wex, H., Niedermeier, D., Hart-
mann, S., Clauss, T., Stratmann, F., Reitz, P., Schneider, J., and Sierau, B.: Irreversible loss
of ice nucleation active sites in mineral dust particles caused by sulphuric acid condensation,
20 *Atmos. Chem. Phys.*, 10, 11471–11487, doi:10.5194/acp-10-11471-2010, 2010.
- Tegen, I., Lacis, A. A., and Fung, I.: The influence on climate forcing of mineral aerosols from
disturbed soils, *Nature*, 380, 419–422, doi:10.1038/380419a0, 1996.
- Tewari, M., Chen, F., Kusaka, H., and Miao, S.: *Coupled WRF/Unified Noah/urban-canopy mod-
eling system*, NCAR WRF Documentation, NCAR, Boulder, 1–22, 2007.
- 25 Twomey, S.: Pollution and planetary albedo, *Atmos. Environ.*, 8, 1251–1256, doi:10.1016/0004-
6981(74)90004-3, 1974.
- Yang, F.: *Radiative forcing and climate impact of the Mount Pinatubo volcanic eruption*, PhD
thesis, University of Illinois at Urbana-Champaign, Urbana-Champaign, USA, 2000.
- Yang, M., Howell, S. G., Zhuang, J., and Huebert, B. J.: Attribution of aerosol light absorp-
tion to black carbon, brown carbon, and dust in China – interpretations of atmospheric mea-
30 surements during EAST-AIRE, *Atmos. Chem. Phys.*, 9, 2035–2050, doi:10.5194/acp-9-2035-
2009, 2009.

**Implementation of
warm-cloud
processes in
a source-oriented
WRF/Chem model**

H.-H. Lee et al.

Title Page

Abstract

Introduction

Conclusions

References

Tables

Figures

◀

▶

◀

▶

Back

Close

Full Screen / Esc

Printer-friendly Version

Interactive Discussion

Ying, Q. and Kleeman, M. J.: Effects of aerosol UV extinction on the formation of ozone and secondary particulate matter, *Atmos. Environ.*, 37, 5047–5068, 2003.

Ying, Q., Lu, J., Allen, P., Livingstone, P., Kaduwela, A., and Kleeman, M.: Modeling air quality during the California regional PM₁₀/PM_{2.5} air quality study (CRPAQS) using the UCD/CIT source-oriented air quality model – Part I: base case model results, *Atmos. Environ.*, 42, 8954–8966, doi:10.1016/j.atmosenv.2008.05.064, 2008.

Zaveri, R. A., Easter, R. C., Fast, J. D., and Peters, L. K.: Model for simulating aerosol interactions and chemistry (MOSAIC), *J. Geophys. Res.-Atmos.*, 113, D13204, doi:10.1029/2007jd008782, 2008.

Zaveri, R. A., Barnard, J. C., Easter, R. C., Riemer, N., and West, M.: Particle-resolved simulation of aerosol size, composition, mixing state, and the associated optical and cloud condensation nuclei activation properties in an evolving urban plume, *J. Geophys. Res.-Atmos.*, 115, D17210, doi:10.1029/2009jd013616, 2010.

Zhang, H., DeNero, S. P., Joe, D. K., Lee, H.-H., Chen, S.-H., Michalakes, J., and Kleeman, M. J.: Development of a source oriented version of the WRF/Chem model and its application to the California regional PM₁₀/PM_{2.5} air quality study, *Atmos. Chem. Phys.*, 14, 485–503, doi:10.5194/acp-14-485-2014, 2014.

Implementation of warm-cloud processes in a source-oriented WRF/Chem model

H.-H. Lee et al.

Title Page

Abstract

Introduction

Conclusions

References

Tables

Figures

◀

▶

◀

▶

Back

Close

Full Screen / Esc

Printer-friendly Version

Interactive Discussion

Table 1. Chemical species that are carried in the AQC/CLDAQC “species” dimension. All species are in concentrations ($\mu\text{g m}^{-3}$) except for the last two elements (i.e., 39 and 40), which carry the number concentration ($\# \text{m}^{-3}$) and radius (m).

Chemical species	Chemical species
1 EC	21 SOA from lumped Alkane 1
2 OC	22 SOA from lumped Alkane 2
3 NA	23 SOA from lumped Aromatic 1
4 CL	24 SOA from lumped Aromatic 2
5 N3	25 SOA from lumped Aromatic 1
6 S6	26 SOA from lumped Aromatic 2
7 N5	27 SOA from lumped Aromatic 1
8 Other	28 SOA from lumped Aromatic 2
9 Metal	29 SOA from lumped Alkene 1
10 Unknown	30 SOA from lumped Alkene 2
11 CU1	31 SOA from lumped Alpha Pinene 1
12 CU2	32 SOA from lumped Alpha Pinene 2
13 MN2	33 SOA from lumped Beta Pinene 1
14 MN3	34 SOA from lumped Beta Pinene 2
15 FE2	35 SOA from lumped Toluene 1
16 FE3	36 SOA from lumped Toluene 2
17 S4	37 Hydrogen Ion
18 Air (hollow sea salt particles)	38 Water
19 NO3	39 Number Concentration
20 Non-explicit SOA	40 Particle Mean Volume Radius

Implementation of warm-cloud processes in a source-oriented WRF/Chem model

H.-H. Lee et al.

Title Page

Abstract

Introduction

Conclusions

References

Tables

Figures



Back

Close

Full Screen / Esc

Printer-friendly Version

Interactive Discussion

Table 2. California Ambient Air Quality Data (CAAQD) station information.

Station ID	Station name	Longitude (°)	Latitude (°)
1	San Jose-Jackson Street	-121.89	37.35
2	Bakersfield-5558 Cal. Avenue	-119.06	35.36
3	Fresno-1st Street	-119.77	36.78
4	Modesto-14th Street	-120.99	37.64
5	Visalia-N Church Street	-119.29	36.33
6	Sacramento-T Street	-121.49	38.57

Implementation of warm-cloud processes in a source-oriented WRF/Chem model

H.-H. Lee et al.

Title Page

Abstract

Introduction

Conclusions

References

Tables

Figures

◀

▶

◀

▶

Back

Close

Full Screen / Esc

Printer-friendly Version

Interactive Discussion

Table 3. Numerical experiment designs for this study.

Experiments	Description
S_ARon_CRmod	Source-Oriented aerosols with aerosol direct effect calculation on and modified cloud radiation parameterization
S_ARon_CRorig	Source-Oriented aerosols with aerosol direct effect calculation on and original cloud radiation parameterization
S_ARoff_CRmod	Source-Oriented aerosols with aerosol direct effect calculation off and modified cloud radiation parameterization
I_ARon_CRmod	Internal mixing aerosols with aerosol direct effect calculation on and modified cloud radiation parameterization

Implementation of warm-cloud processes in a source-oriented WRF/Chem model

H.-H. Lee et al.

Table 4. Hourly bias mean and standard deviation (SD) in day time and night time of 2 m temperature ($T2$, °C), water vapor mixing ratio ($Q2$, g kg⁻¹), and net downward shortwave radiative flux (NSF, W m⁻²) between all experiments and observation from 16 to 18 January 2011. $T2$ and $Q2$ are calculated using 24 surface stations and NSF is calculated using 42 CIMIS stations shown in Fig. 4.

	S_ARon_CRmod		S_ARon_CRorig		S_ARoff_CRmod		I_ARon_CRmod	
Daytime	Bias mean	SD	Bias mean	SD	Bias mean	SD	Bias mean	SD
$T2$	-1.76	1.27	-1.72	1.32	-1.63	1.33	-2.01	1.09
$Q2$	-0.56	0.34	-0.56	0.36	-0.54	0.35	-0.57	0.32
NSF	13.91	53.18	14.40	58.00	18.81	58.78	8.68	50.03
Nighttime	Bias mean	SD	Bias mean	SD	Bias mean	SD	Bias mean	SD
$T2$	-2.22	0.92	-2.21	0.95	-2.19	0.93	-2.30	0.87
$Q2$	-0.88	0.41	-0.87	0.42	-0.88	0.42	-0.89	0.41
NSF	-	-	-	-	-	-	-	-

Title Page

Abstract

Introduction

Conclusions

References

Tables

Figures

◀

▶

◀

▶

Back

Close

Full Screen / Esc

Printer-friendly Version

Interactive Discussion

Implementation of warm-cloud processes in a source-oriented WRF/Chem model

H.-H. Lee et al.

Table 6. Ratio of AQC number concentration for each bin/source to the total, averaged within the first five model layers during 16 to 18 January 2011.

	Wood smoke	Gasoline	Diesel	Meat cooking	Others	Source-oriented	Internal
Bin1	28.92 %	1.00 %	4.25 %	0.84 %	10.39 %	45.40 %	48.89 %
Bin2	9.12 %	0.38 %	1.48 %	0.60 %	38.64 %	50.22 %	46.74 %
Bin3	0.19 %	0.01 %	0.03 %	0.02 %	3.03 %	3.28 %	3.26 %
Bin4	0.00 %	0.00 %	0.00 %	0.00 %	0.17 %	0.18 %	0.21 %
Bin5	0.00 %	0.00 %	0.00 %	0.00 %	0.02 %	0.02 %	0.02 %
Bin6	0.00 %	0.00 %	0.00 %	0.00 %	0.00 %	0.00 %	0.00 %
Bin7	0.00 %	0.00 %	0.00 %	0.00 %	0.00 %	0.00 %	0.00 %
Bin8	0.00 %	0.00 %	0.00 %	0.00 %	0.91 %	0.91 %	0.88 %

Title Page

Abstract

Introduction

Conclusions

References

Tables

Figures

◀

▶

◀

▶

Back

Close

Full Screen / Esc

Printer-friendly Version

Interactive Discussion

Implementation of warm-cloud processes in a source-oriented WRF/Chem model

H.-H. Lee et al.

Table 7. Hourly bias mean and root-mean-square-difference of cloud water mixing ratio (Q_c), cloud droplet number (Q_n), surface skin temperature (SKT), net shortwave flux (NSF), latent heat flux (LH) and sensible heat flux (SH) between internally mixed (I_ARon_CRmod) and source-oriented (S_ARon_CRmod) experiments (internally mixed – source-oriented) during 16 to 18 January 2011.

	Bias mean	Root-mean-square-difference
Q_c^* (g m^{-3})	1.19×10^{-2}	4.16×10^{-2}
Q_n^* ($\# \text{ m}^{-3}$)	6.24×10^7	2.64×10^8
SKT (K)	-0.15	0.57
NSF (W m^{-2})	-6.02	13.30
LH (W m^{-2})	-0.61	2.75
SH (W m^{-2})	-0.36	5.24

* Averaged within the first five model layers.

Title Page

Abstract

Introduction

Conclusions

References

Tables

Figures

◀

▶

◀

▶

Back

Close

Full Screen / Esc

Printer-friendly Version

Interactive Discussion

Implementation of warm-cloud processes in a source-oriented WRF/Chem model

H.-H. Lee et al.

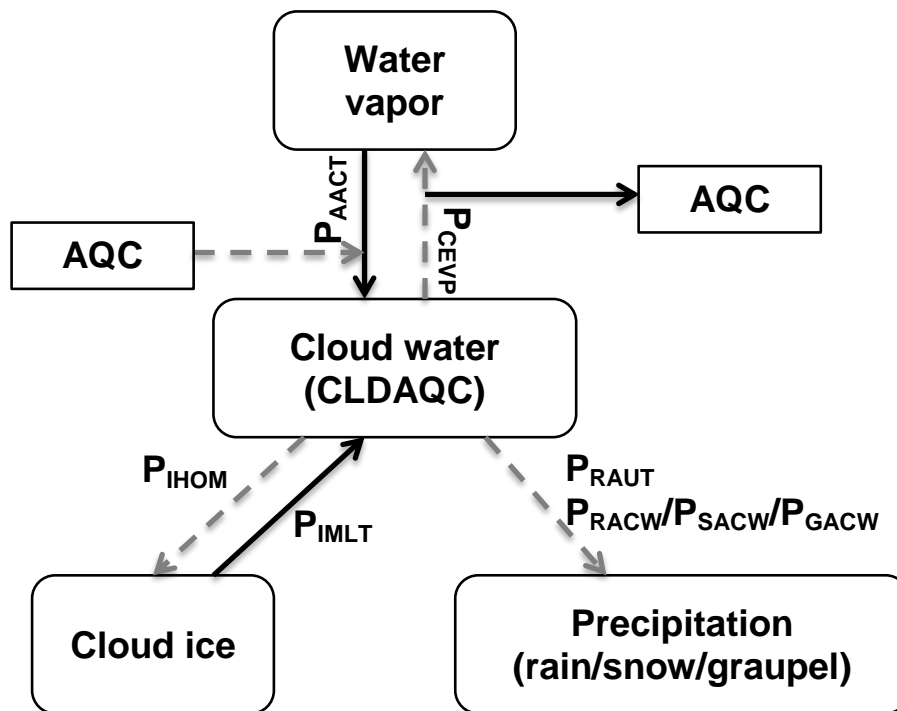


Figure 1. Cloud physics processes that are involved with cloud particles in the SOWC model with a 6-D aerosol variable (AQC) and a 6-D cloud variable (CLDAQC) included. Black solid arrow and grey dashed arrow indicate the source and the sink processes of cloud water and 6-D CLDAQC, as well as 6-D AQC, respectively.

Title Page	
Abstract	Introduction
Conclusions	References
Tables	Figures
◀	▶
◀	▶
Back	Close
Full Screen / Esc	
Printer-friendly Version	
Interactive Discussion	



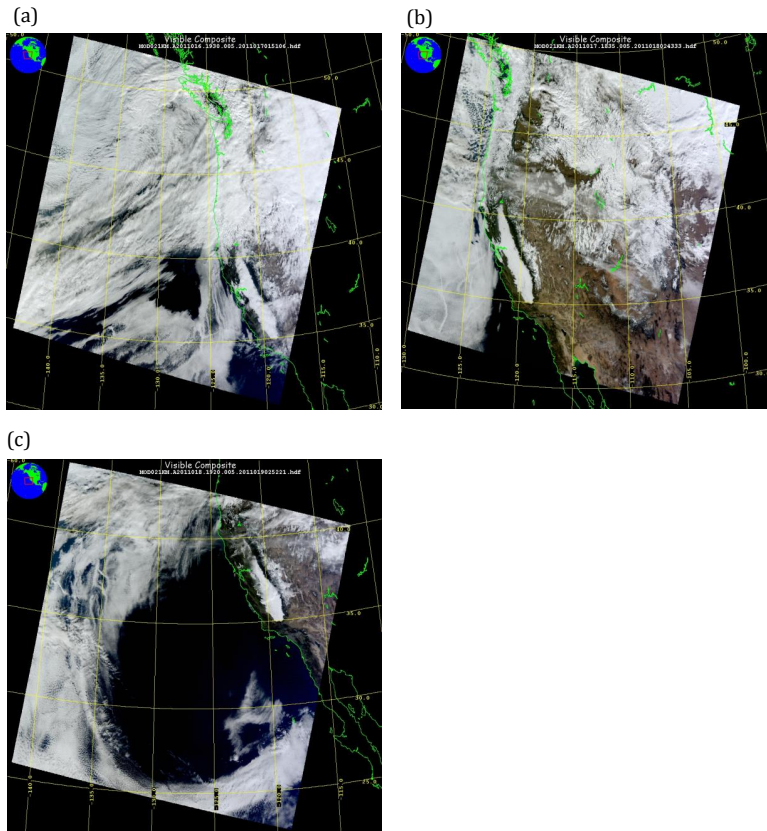


Figure 2. MODIS true color images at (a) 19:30 UTC, 16 January, (b) 18:35 UTC, 17 January, and (c) 19:20 UTC, 18 January 2011 from Satellite Terra.

Implementation of warm-cloud processes in a source-oriented WRF/Chem model

H.-H. Lee et al.

Title Page	
Abstract	Introduction
Conclusions	References
Tables	Figures
◀	▶
◀	▶
Back	Close
Full Screen / Esc	
Printer-friendly Version	
Interactive Discussion	



Implementation of warm-cloud processes in a source-oriented WRF/Chem model

H.-H. Lee et al.

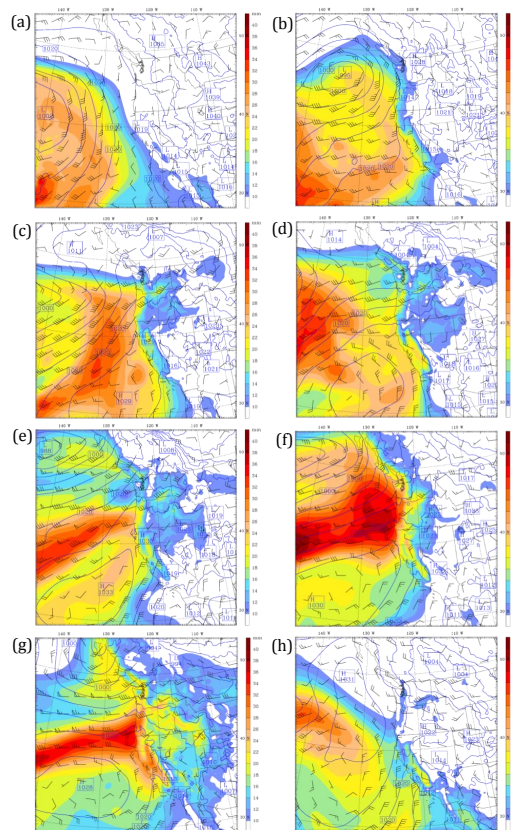


Figure 3. The column integrated water vapor (shaded; mm), 850 hPa wind vector, and sea level pressure (contours; hPa) from ECMWF Interim reanalysis at **(a)** 00:00 UTC (4:00 p.m. LT) 11 January, **(b)** 00:00 UTC, 12 January, **(c)** 00:00 UTC, 13 January, **(d)** 00:00 UTC, 14 January, **(e)** 00:00 UTC, 15 January, **(f)** 00:00 UTC, 16 January, **(g)** 00:00 UTC, 17 January, and **(h)** 00:00 UTC, 18 January 2011.

[Title Page](#)[Abstract](#)[Introduction](#)[Conclusions](#)[References](#)[Tables](#)[Figures](#)[◀](#)[▶](#)[◀](#)[▶](#)[Back](#)[Close](#)[Full Screen / Esc](#)[Printer-friendly Version](#)[Interactive Discussion](#)

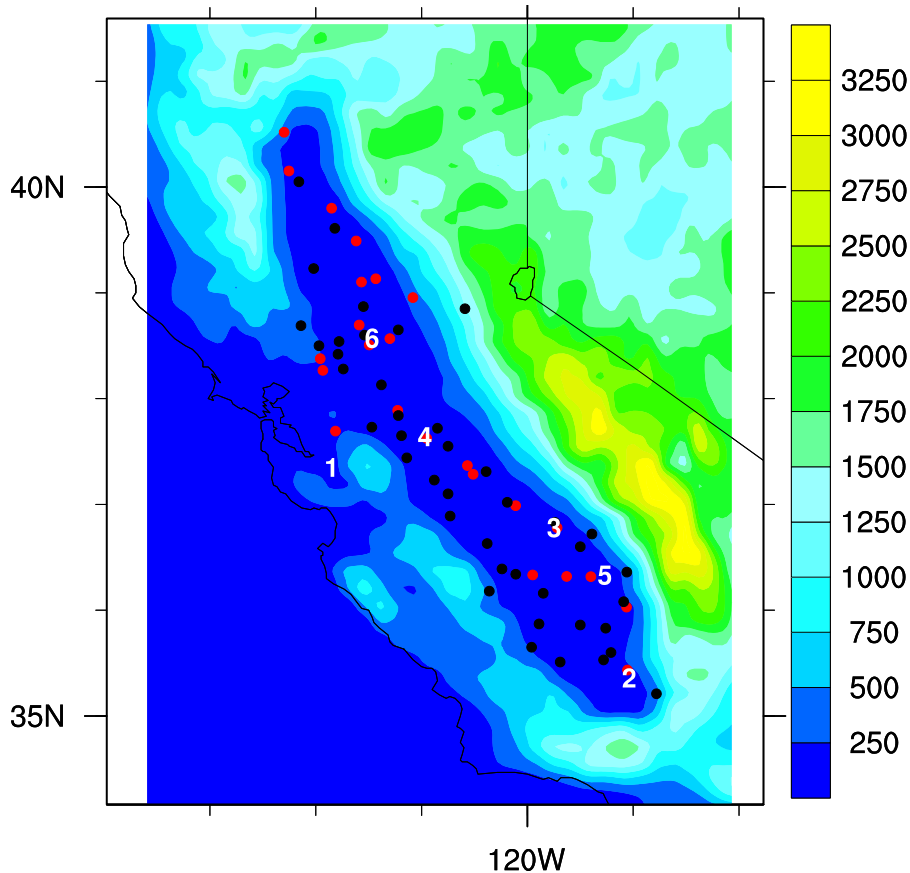


Figure 4. NOAA's National Climatic Data Center (NCDC; 24 stations, red dots), California Irrigation Management Information System (CIMIS; 42 stations, black dots) and California Ambient Air Quality Data (6 stations, numbers corresponding to Table 2 station ID) measurement locations. Shaded is terrain height in m.

Implementation of warm-cloud processes in a source-oriented WRF/Chem model

H.-H. Lee et al.

Title Page	
Abstract	Introduction
Conclusions	References
Tables	Figures
◀	▶
◀	▶
Back	Close
Full Screen / Esc	
Printer-friendly Version	
Interactive Discussion	



**Implementation of
warm-cloud
processes in
a source-oriented
WRF/Chem model**

H.-H. Lee et al.

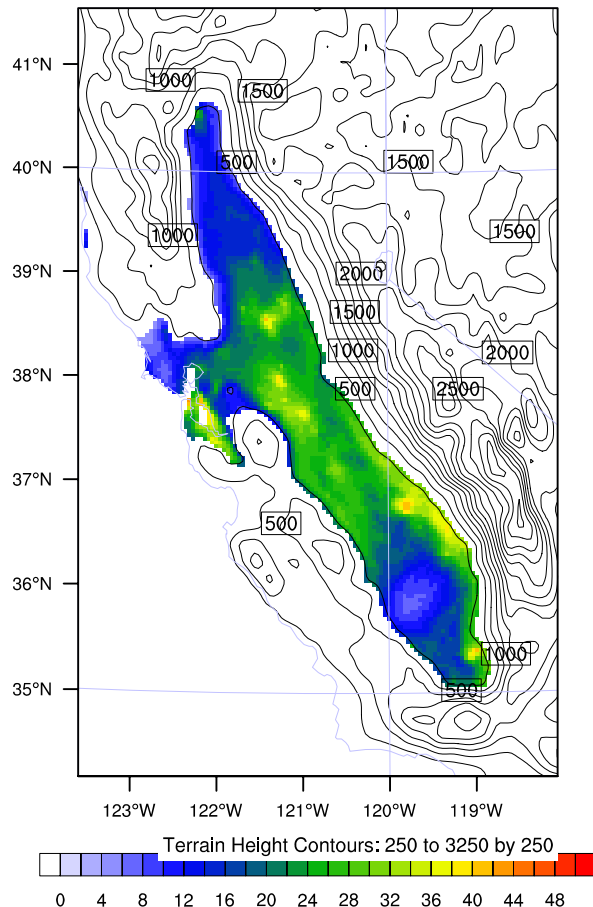


Figure 5. The 72 h averaged (16 to 18 January 2011) AQC number concentration averaged over the first five model layers from the experiment S_ARon_CRmod in units of $10^8 \# \text{m}^{-3}$. Contours are terrain heights in m.

Implementation of warm-cloud processes in a source-oriented WRF/Chem model

H.-H. Lee et al.

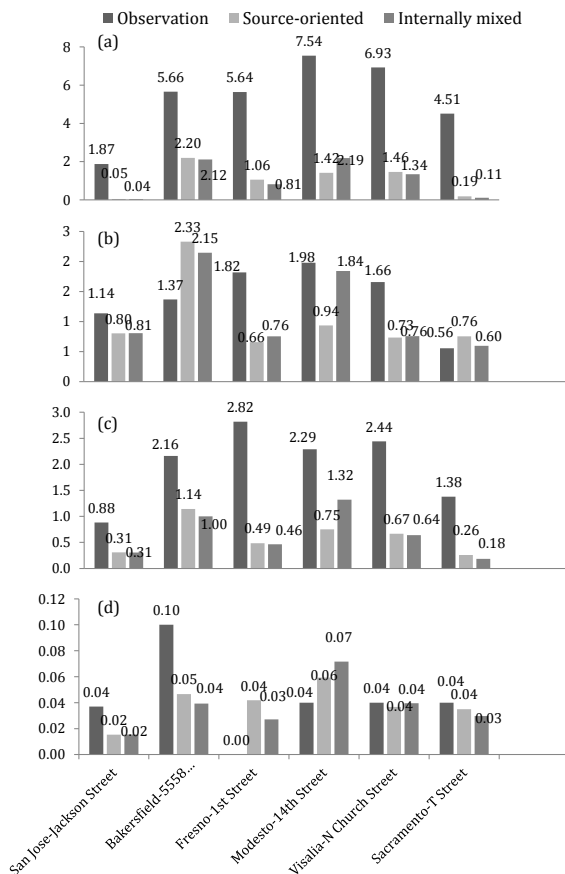


Figure 6. Comparison of (a) Nitrate (NO_3^-), (b) Sulfate (SO_4^{2-}), (c) Ammonium (NH_4^+), and (d) Soluble Sodium (Na^+) between simulated source-oriented experiment (S_ARon_CRmod), internally mixed experiment (I_ARon_CRmod) and the observed concentrations of airborne particles on 18 January 2011. Units are $\mu\text{g m}^{-3}$.

Title Page

Abstract Introduction

Conclusions References

Tables Figures

◀ ▶

◀ ▶

Back Close

Full Screen / Esc

Printer-friendly Version

Interactive Discussion



Implementation of
warm-cloud
processes in
a source-oriented
WRF/Chem model

H.-H. Lee et al.

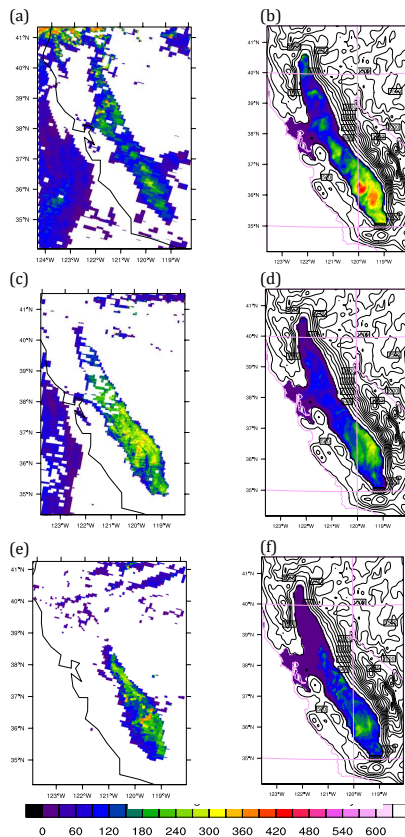


Figure 7. Liquid water path (LWP) (gm^{-2}) from MODIS Level 2 cloud products **(a)**, **(c)** and **(e)** and from the SOWC model with aerosol feedback on and modified cloud–radiation scheme (S_ARon_CRmod; **(b)**, **(d)** and **(e)**). **(a)** and **(b)** are at 19:00 UTC, 16 January 2011. **(c)** and **(d)** are at 18:00 UTC, 17 January 2011. **(e)** and **(f)** are at 19:00 UTC, 18 January 2011. Contours in **(b)**, **(d)** and **(e)** are terrain heights in m.

Implementation of
warm-cloud
processes in
a source-oriented
WRF/Chem model

H.-H. Lee et al.

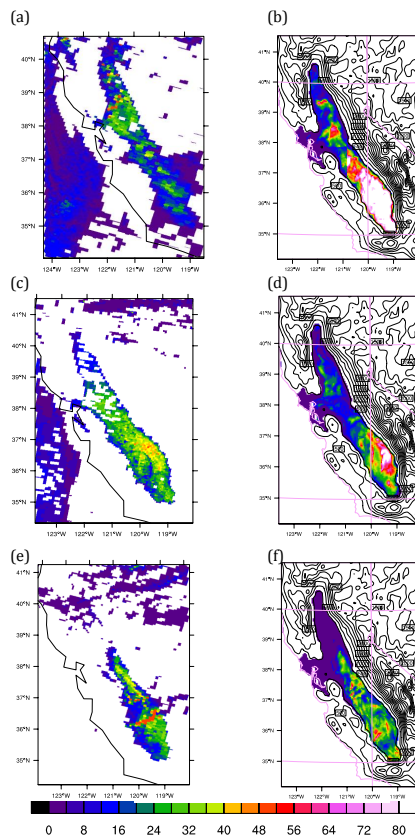


Figure 8. Same as Fig. 5 but cloud optical thickness (COT) (dimensionless).

Implementation of
warm-cloud
processes in
a source-oriented
WRF/Chem model

H.-H. Lee et al.

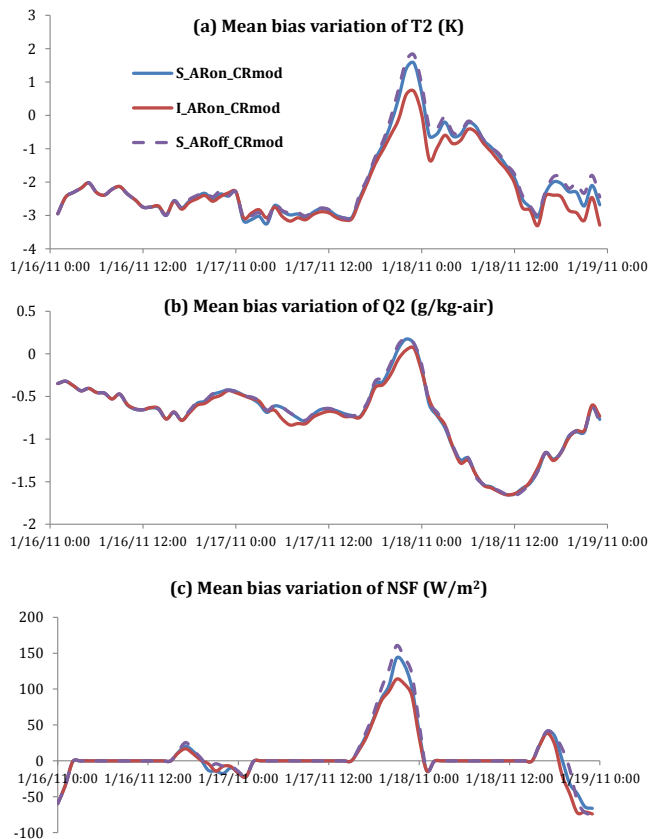


Figure 9. Mean bias variation of **(a)** 2 m temperature (T_2), **(b)** 2 m water vapor mixing ratio (Q_2), and **(c)** surface net downward shortwave radiative flux (NSF) between observations and model simulation from 16 to 18 January 2011 for S_ARon_CRmod (blue lines), S_ARoff_CRmod (purple lines) and I_ARon_CRmod (red lines) experiments.

Implementation of warm-cloud processes in a source-oriented WRF/Chem model

H.-H. Lee et al.

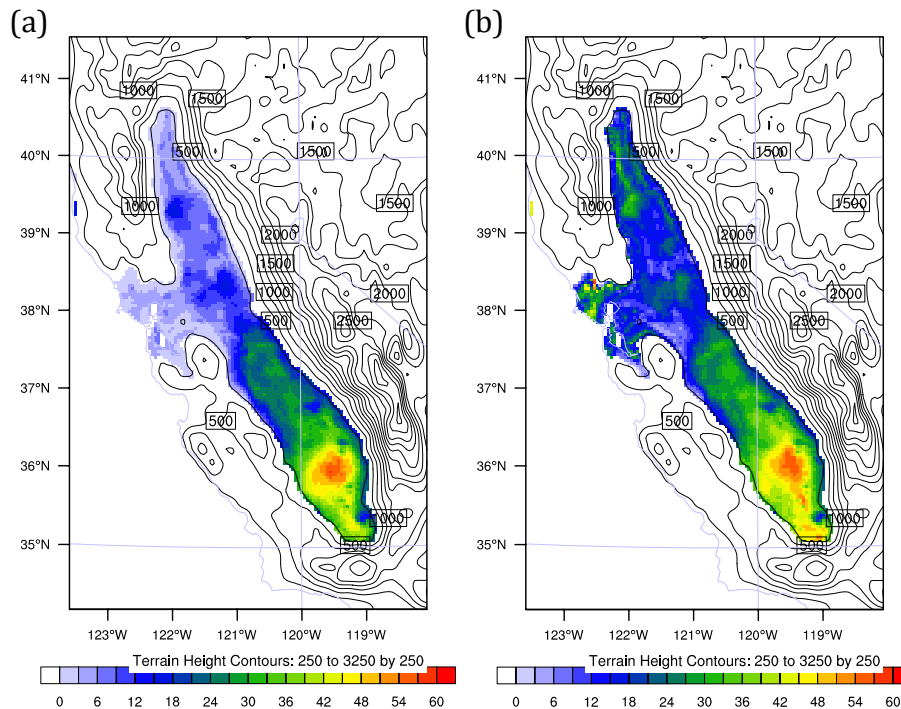


Figure 10. N_{CCN}/N_{CN} ratio for (a) S_ARon_CRmod (source-oriented experiment) and (b) I_ARon_CRmod (internally mixed experiment) averaged within the first five model layers. The ratio is hourly average during 16 to 18 January 2011. Contours are terrain heights in m.

Title Page

Abstract

Introduction

Conclusions

References

Tables

Figures

◀

▶

◀

▶

Back

Close

Full Screen / Esc

Printer-friendly Version

Interactive Discussion

Implementation of warm-cloud processes in a source-oriented WRF/Chem model

H.-H. Lee et al.

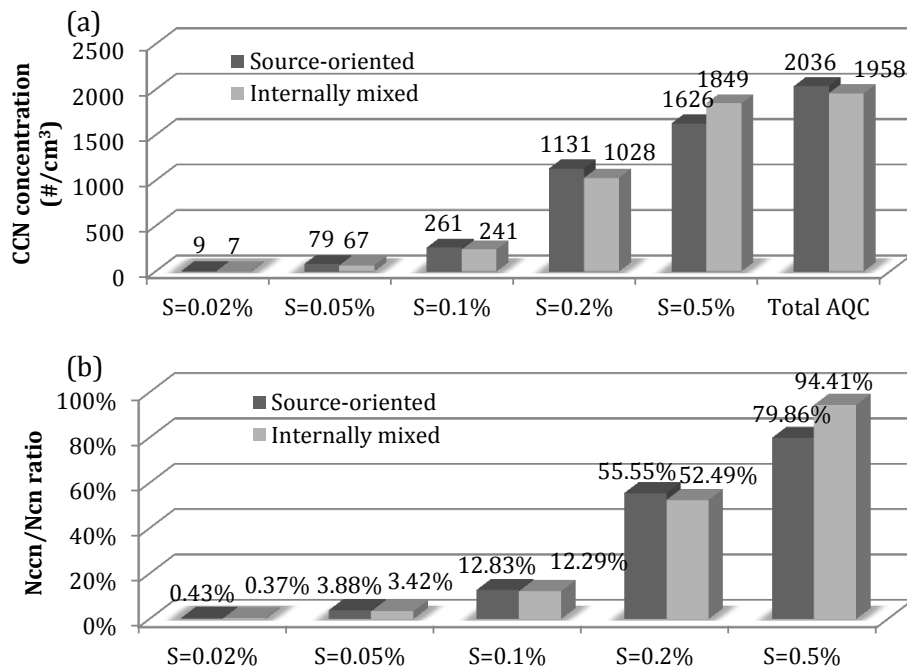


Figure 11. (a) 72 h averaged CCN concentration at supersaturation of 0.02, 0.05, 0.1, 0.2, 0.5% and total AQC concentration with units in # cm⁻³. (b) N_{CCN}/N_{CN} ratio at 5 corresponding supersaturation. Dark gray is source-oriented experiment and light gray represents internally mixed experiment. Results are average values using data within the first five model layers.

Title Page

Abstract Introduction

Conclusions References

Tables Figures

◀ ▶

◀ ▶

Back Close

Full Screen / Esc

Printer-friendly Version

Interactive Discussion



Implementation of warm-cloud processes in a source-oriented WRF/Chem model

H.-H. Lee et al.

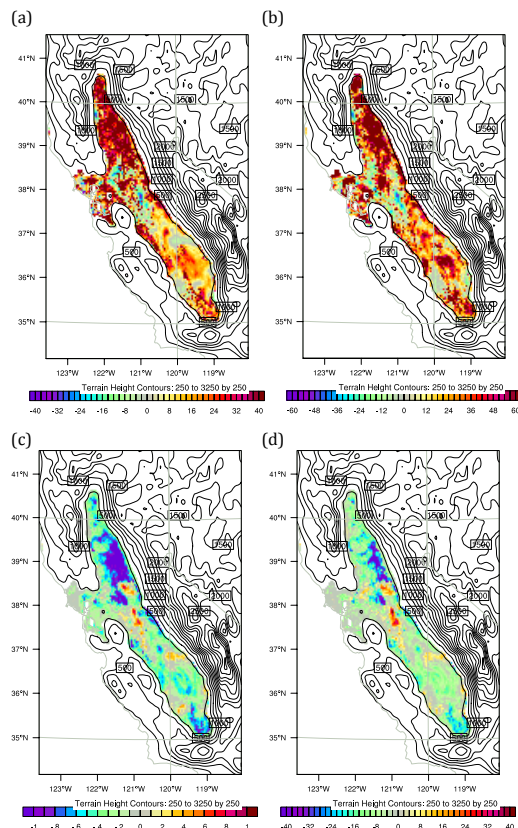


Figure 12. Relative change ((internally mixed – source-oriented)/source-oriented $\times 100\%$) in the daytime averaged predictions during 16 to 18 January 2011 for **(a)** the ratio of cloud water mixing ratio, **(b)** cloud droplet number and absolute difference (internally mixed – source-oriented) in **(c)** surface skin temperature (K) and **(d)** net shortwave radiation ($W m^{-2}$). **(a)** and **(b)** are average values using data within the first five model layers. Contours are terrain heights in m.

**Implementation of
warm-cloud
processes in
a source-oriented
WRF/Chem model**

H.-H. Lee et al.

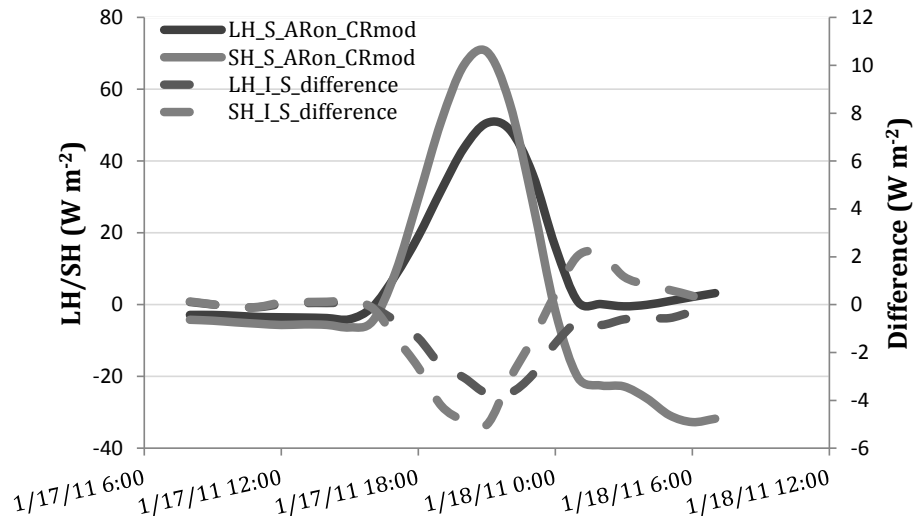


Figure 13. Area average of latent heat flux (LH) and sensible heat flux (SH) over the Central Valley in S_ARon_CRmod and the average difference between I_ARon_CRmod and S_ARon_CRmod from 08:00 UTC, 17 January (00:00 LT) to 07:00 UTC, 18 January (23:00 LT).